

ManiFest: Manifold Deformation for Few-shot Image Translation

Fabio Pizzati
Inria, Vislab

fabio.pizzati@inria.fr

Jean-François Lalonde
Université Laval

jflalonde@gel.ulaval.ca

Raoul de Charette
Inria

raoul.de-charette@inria.fr

Abstract

Most image-to-image translation methods require a large number of training images, which restricts their applicability. We instead propose ManiFest: a framework for few-shot image translation that learns a context-aware representation of a target domain from a few images only. To enforce feature consistency, our framework learns a style manifold between source and proxy anchor domains (assumed to be composed of large numbers of images). The learned manifold is interpolated and deformed towards the few-shot target domain via patch-based adversarial and feature statistics alignment losses. All of these components are trained simultaneously during a single end-to-end loop. In addition to the general few-shot translation task, our approach can alternatively be conditioned on a single exemplar image to reproduce its specific style. Extensive experiments demonstrate the efficacy of ManiFest on multiple tasks, outperforming the state-of-the-art on all metrics and in both the general- and exemplar-based scenarios. Our code is available at <https://github.com/cv-rits/ManiFest>.

1. Introduction

Image-to-image translation (i2i) frameworks are gaining more and more traction on multiple applications such as domain adaptation for autonomous driving [22, 44] as well as photo editing [35, 36]. While these methods have shown promising results, most of them require the availability of large-scale training datasets to generate realistic samples, and as such they are restricted to domains where large quantities of images are available. Unfortunately, it is unrealistic to impose significant data collection constraints every time a new i2i scenario is pursued. In addition to the complex logistics involved in acquiring large quantities of images, some scenarios may be rare (e.g., auroras) or dangerous (e.g., erupting volcanoes) thereby preventing the straightforward gathering of sufficient training data. Existing methods have been proposed to alleviate the requirement for large datasets, but they mostly show realistic results in highly structured environments such as face translation [28, 43].

In this context, we propose ManiFest, a framework for

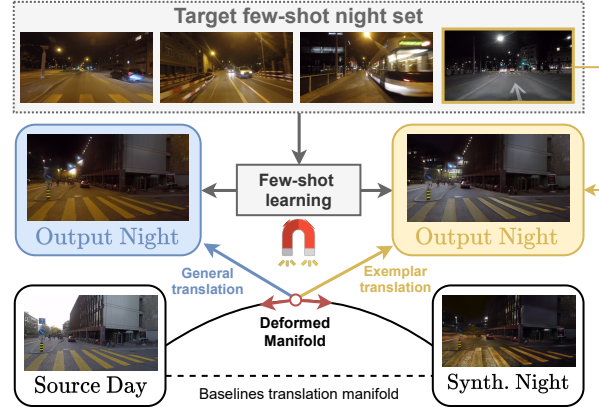


Figure 1. Overview of ManiFest, which translates images from a source domain (here, Day) to a few-shot target (Night). Our framework learns a manifold between *anchor* domains, in the example spanning the translation between Day and Synthetic Nighttime. Our system deforms the manifold by injecting the few-shot domain information between anchor style representations, and further departs from the deformed manifold by learning to approximate the target domain *general* appearance, or to reproduce the style of a particular *exemplar*.

few-shot image-to-image translation which is shown to be robust to highly unstructured transformations such as adverse weather generation or night rendering. Our approach, illustrated in Fig. 1, departs from the observation that features consistency is crucial for i2i [30] and that few-shot domain offers little cues to train efficiently without overfitting [33]. Hence, rather than directly addressing the i2i few-shot, ManiFest deforms a stable learned manifold towards our few-shot target, and leverages style transfer and patch-based training to enable few-shot learning. Our framework is beneficial for several applications since it learns to both: translate to a single *general* style approximating the entire few-shot set (e.g., for photo editing); or reproduce any specific *exemplar* from the set for increased variability (e.g., for domain adaptation). In short, our contributions are:

- ManiFest, a few-shot image translation system based on feature consistency by weighted manifold interpolation

(WMI) and local-global few-shot loss (LGFS).

- We propose the first mechanism to perform both *general* and *exemplar* few-shot image translation by using our novel general/exemplar residual module (GERM).
- Our framework outperforms previous work on adverse weather and low-light few-shot image translation tasks. We also present qualitative evaluations on rare (auroras) and dangerous (volcanoes) events.

2. Related work

Image-to-image translation (i2i) Although the early i2i translation methods required paired data [14, 64], cycle-consistency [27, 63] or recent alternatives with contrastive learning [34] have lifted such constraint. Many approaches separate style and content to enable multi-modal or multi-target translations [5, 13, 16, 18, 57], while others use additional strategies to increase scene contextual preservation [15, 62]. Translation networks can be conditioned on a variety of additional information, including semantics [4, 19, 24, 30, 41, 48, 65, 66], instances [32], geometry [55], models [11, 38–40, 50], low-resolution inputs [1] or exemplar images [30, 58, 59]. Still, all require a large amount of data.

GANs with limited data There have been several attempts to overcome the large data requirement for training GANs. Some use transfer learning [49] to adapt previously-trained networks to new few-shot tasks [23, 54]. In particular, [33] uses a patch-based discriminator to generalize to few-shot domains. However, these methods are designed for generative networks and do not immediately apply to i2i. Another line of work focuses on the limited data scenario [2, 17, 37, 61], but usually performs poorly when very few (10–15) images are used for training. Others exploit additional knowledge to enable few-shot or zero-shot learning, such as pose-appearance decomposition [53], image conditioning [8] or textual inputs [26]. FUNT [28] and COCO-FUNIT [43] use few-shot style encoders to adapt the network behavior at inference time. Some use meta-learning to adapt quickly to newly seen domains [25]. Those methods show limited performance on highly unstructured scenarios. [7] exploits geometry for patch-based few-shot training, but only on limited domains with specific characteristics.

Neural style transfer Style transfer could be seen as an instance of few-shot i2i, where the goal is to combine the content of an image with the style of another [9]. This often results in distortions, which some work tried to mitigate [29]. The first examples for style transfer with arbitrary input style images are in [12, 20]. Others try to transfer styles in a photo-realistic manner by using a smoothing step [21] or by using wavelet transforms [56]. While these methods provide good results in some controlled scenarios, they may fail to understand the contextual mapping between source and style images elements (e.g. sky, buildings, etc.) which we learn more accurately.

3. ManiFest

The few-shot i2i task consists in learning a $\mathcal{S} \mapsto \mathcal{T}$ mapping between images of source domain \mathcal{S} and target domain \mathcal{T} containing few training samples (e.g., $|\mathcal{T}| \leq 25$). Fig. 2 presents an overview of our approach. We learn a style manifold in a standard multi-target GAN fashion (Sec. 3.1) from a set of so-called *anchor* domains \mathbb{A} with a large amount of training data. Our Weighted Manifold Interpolation (WMI, Sec. 3.2) exploits interpolation to increase translated feature consistency. We allow to further depart from the interpolated manifold with the General-Exemplar Residual Module (GERM, Sec. 3.3) which learns a residual image refining the overall appearance. GERM also allows transfer to the *general* few-shot style (learned from the entire few shot set), or to a single *exemplar* as in [30]. We learn \mathcal{T} appearance and inject it in the manifold with the Local-Global Few-Shot loss (LGFS, Sec. 3.4). In the following, *real* images are $s \in \mathcal{S}$, $t \in \mathcal{T}$, and *fake* ones $\tilde{s} \in \mathcal{T}$ where \tilde{s} is our output.

3.1. Multi-target i2i

Instead of learning $\mathcal{S} \mapsto \mathcal{T}$ directly, we assume the availability of a set $\mathbb{A} = \{\mathcal{A}_{\text{id}}, \mathcal{A}_m\}$ of *anchor* domains for which we have lots of data available (equivalent to the “base” categories in few-shot image classification, e.g. [3]). By construction, one anchor is always the identity domain ($\mathcal{A}_{\text{id}} = \mathcal{S}$), while the other (\mathcal{A}_m) contains images easier to collect with respect to \mathcal{T} , for example synthetic images or images from existing datasets. We formalize the multi-target image translation problem as learning the $\mathcal{S} \mapsto \mathbb{A}$ mapping.

At training time, we assume that the anchor domains have corresponding latent style representations [13] $\{z_{\text{id}}, z_m\}$ and translate to a randomly selected domain $c \in \{\text{id}, m\}$ with

$$z_c = \sum_{i \in \{\text{id}, m\}} \llbracket c = i \rrbracket z_i, \quad \tilde{s}_c = G_{z_c}(E(s)), \quad (1)$$

where $\llbracket \cdot \rrbracket$ are the Iverson brackets, and G_{z_c} the style injection of z_c into G as in [13]. The multi-target discriminator D_{mt} employs adversarial losses $\mathcal{L}_{\text{adv}}^G$ and $\mathcal{L}_{\text{adv}}^D$ to force fake images \tilde{s}_c to resemble $a_c \in \mathcal{A}_c$. Additional training details are in the supp. material.

3.2. Weighted Manifold Interpolation (WMI)

Our intuition is that encoding \mathcal{T} between the linearly interpolated style representations of \mathbb{A} should enforce feature consistency in \mathcal{T} . For instance, assuming $\mathcal{S} = \text{day}$, $\mathcal{T} = \text{night}$, $\mathcal{A}_m = \text{synthetic night}$, the network will be provided with the information that all sky pixels should be darkened together.

In practice, we learn weights $w = \{w_{\text{id}}, w_m\}$ which sum to 1 and encode an image \tilde{s}_w with feature consistency by interpolating the anchors style representations:

$$z_w = \sum_{i \in \{\text{id}, m\}} w_i z_i, \quad \tilde{s}_w = G_{z_w}(E(s)). \quad (2)$$

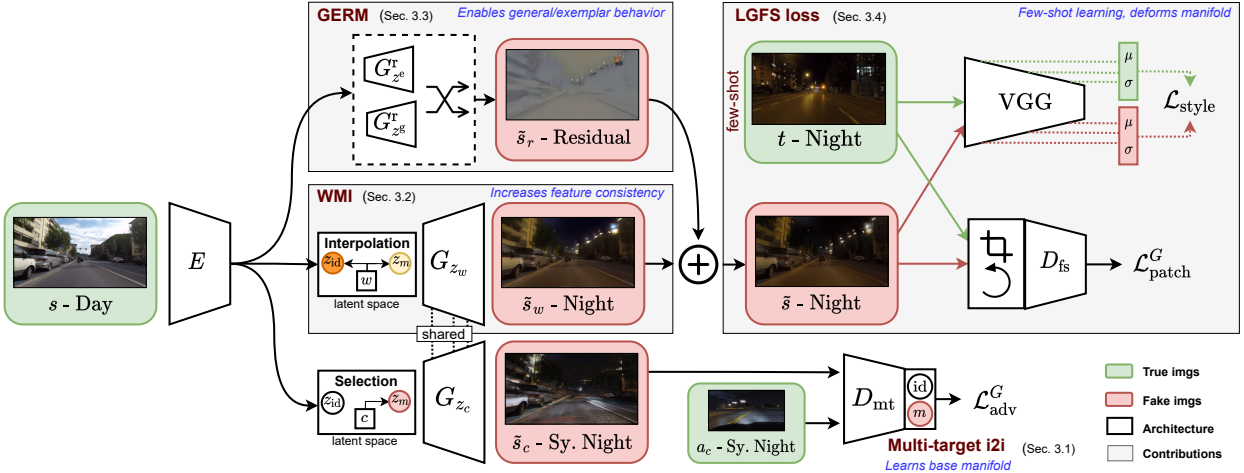


Figure 2. ManiFest architecture. The encoded image representation $E(s)$ is separated in content and style codes and translated to the few-shot domain by injecting \mathcal{T} on a manifold spanned by auxiliary anchors, with additional feature consistency provided by WMI. We learn the anchor manifold in a multi-target i2i setting. We correct the output by using residuals estimated by the GERM (Fig. 3). We train with our LGFS loss, based on statistics alignment and patch-based adversarial learning, which deforms the manifold and injects \mathcal{T} in it.

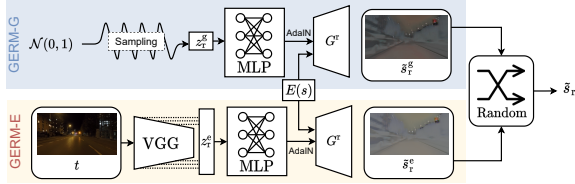


Figure 3. GERM-based residuals. We perform either *exemplar*- or *general*-based transformations on the few-shot set by learning residuals conditioned on extracted statistics or noise, respectively.

Learning w allows us to determine the point in the \mathbb{A} manifold which is most consistent with \mathcal{T} . This point is determined with help from the LGFS loss (Sec. 3.4).

3.3. General-Exemplar Residual Module (GERM)

We allow deviations from the \mathbb{A} manifold by learning a residual image \tilde{s}_r , which helps encode characteristics from \mathcal{T} that are absent in \mathbb{A} . This is done by processing the input image features $E(s)$ with a generator G^r such that

$$\tilde{s}_r = G^r(E(s)), \quad \text{and} \quad \tilde{s} = \tilde{s}_w + \tilde{s}_r. \quad (3)$$

We provide two ways of generating the residual image, *i.e.*, $\tilde{s}_r \in \{\tilde{s}_r^e, \tilde{s}_r^g\}$. In both cases, we draw inspiration from AdaIN style injection [13] and randomly condition the injected parameters either on extracted feature statistics (*exemplar*), or on random gaussian noise (*general*).

To reproduce the style of a specific image $t \in \mathcal{T}$ as in [30], we provide an *exemplar* residual (“GERM-E” in Fig. 3) by conditioning on t . In this case,

$$\tilde{s}_r^e = (\mu_k(t), \sigma_k(t))|_{k=1}^K, \quad \tilde{s}_r^g = G_{z_r^g}^r(E(s)), \quad (4)$$

where $\mu_k(\cdot) = \mu(\phi_k(\cdot))$ and $\sigma_k(\cdot) = \sigma(\phi_k(\cdot))$ are mean and variance of the k -th out of K layer outputs ϕ_k of a pretrained VGG network [12], and $\| \cdot \|$ is the concatenation operator.

We identify as *general* residual some \tilde{s}_r^g which moves the generated image towards \mathcal{T} by mimicking an average style learned from all images in \mathcal{T} . This is illustrated as “GERM-G” in Fig. 3, and, mathematically:

$$z_r^g \sim \mathcal{N}(0, 1), \quad \tilde{s}_r^g = G_{z_r^g}^r(E(s)). \quad (5)$$

3.4. Local-Global Few-Shot loss (LGFS)

The quality of the resulting image \tilde{s} is compared against the few-shot training set \mathcal{T} with a combination of two loss functions. First, we take inspiration from the state-of-the-art of image style transfer where one image is enough for transferring the *global* appearance of the style scene [12]. Our intuition is that feature statistics alignment, vastly used in style transfer, could be less prone to overfitting with respect to adversarial training. So, we align features between \tilde{s} and a target image $t \in \mathcal{T}$ using a style loss as in [12], such as

$$\mathcal{L}_{\text{style}} = \sum_{k=1}^K \|\mu_k(\tilde{s}) - \mu_k(t)\|_2 + \|\sigma_k(\tilde{s}) - \sigma_k(t)\|_2, \quad (6)$$

where (μ_k, σ_k) are the same as in Sec. 3.3. While this is effective in modifying the general image appearance, aligning statistics alone is insufficient to produce realistic outputs. Thus, to provide *local* guidance, *i.e.* on more fine-grained characteristics, we employ an additional discriminator D_{fs} which is trained to distinguish between rotated patches sam-

pled from \tilde{s} and t . We define the adversarial losses [31]:

$$\begin{aligned}\mathcal{L}_{\text{patch}}^G &= \|D_{\text{fs}}(p(\tilde{s})) - 1\|_2, \\ \mathcal{L}_{\text{patch}}^D &= \|D_{\text{fs}}(p(\tilde{s}))\|_2 + \|D_{\text{fs}}(p(t)) - 1\|_2,\end{aligned}\quad (7)$$

where p is a random cropping and rotation function. Note how GERM-E is conditioned on the *same* feature statistics used in the LGFS loss—this is what enables the exemplar behavior of the network. Note the interaction between components, since backpropagating the LGFS loss indeed *deforms* the manifold learned by multi-target i2i in the point identified by WMI, injecting \mathcal{T} between $\{\mathcal{A}_{\text{id}}, \mathcal{A}_m\}$.

3.5. Training strategy

Our framework is fully trained end-to-end and optimizes

$$\begin{aligned}\min_{\Theta(E, G, G^r)} \mathcal{L}_{\text{style}} + \mathcal{L}_{\text{patch}}^G + \mathcal{L}_{\text{adv}}^G \quad &\text{and} \\ \min_{\Theta(D_{\text{fs}}, D_{\text{mt}})} \mathcal{L}_{\text{patch}}^D + \mathcal{L}_{\text{adv}}^D,\end{aligned}\quad (8)$$

where $\Theta(\cdot)$ refers to the network parameters.

We train GERM-G and GERM-E (Sec. 3.3) in alternance by randomly selecting one scenario at each training iteration. For the multi-target settings, we adapt the discriminator of our backbone in a multi-target setup following [5].

4. Experiments

We leverage 4 datasets [6, 42, 44, 45] (Sec. 4.1.1) and 3 translation tasks (Sec. 4.1.2) and evaluate performance against recent baselines [13, 28, 30, 43, 56] (Sec. 4.2). We further demonstrate the benefit of our few-shot translation on a proxy segmentation tasks (Sec. 4.3), and rare few-shot scenarios (Sec. 4.4), and finally ablate our contributions (Sec. 4.5). In all, we use MUNIT [13] as our backbone.

4.1. Training setup

4.1.1 Datasets

ACDC We use ACDC [45] for most of our experiments, using the night/rain/snow/fog conditions with 400/100/500 images for train/val/test respectively, following official splits. For any individual condition, ACDC also includes geolocalized weakly-paired clear weather day images of same splits.

Dark Zurich Similar to ACDC, Dark Zurich (DZ) [44] has daytime images paired with nighttime/twilight conditions. Here, we focus on twilight conditions exclusively and use training images from the GOPRO348 sequence only since it exhibits a distinctive twilight appearance. We split the total 819 image pairs into 25/794 for train/test, respectively.

Cityscapes Cityscapes [6] is used to evaluate ManiFest for training segmentation networks robust to nighttime¹. It includes 2975/500/1525 annotated images for train/val/test.

¹ACDC does not provide annotated daytime clear weather sequences.

VIPER As anchor domains, we employ synthetic images from the VIPER dataset [42], using the condition metadata to define splits. 4137/3090/1305/2018/2817 images are extracted from the VIPER training set for day/night/rain/snow/sunset conditions, respectively.

4.1.2 Tasks and evaluation

We train our framework on three main tasks:

Day \mapsto Night on ACDC daytime (\mathcal{S}) and nighttime (\mathcal{T}).

Clear \mapsto Fog on ACDC daytime (\mathcal{S}) and fog (\mathcal{T}).

Day \mapsto Twilight on DZ daytime (\mathcal{S}) and twilight (\mathcal{T}).

Unless mentioned otherwise, the (synthetic) anchor domains from VIPER are “night” for Day \mapsto Night and Day \mapsto Twilight, and “day” for Clear \mapsto Fog. We evaluate with the FID [10] and LPIPS [60] metrics. While FID compares feature distance globally, LPIPS compares translated source images and the geolocalized paired image in the target dataset. This is beneficial for evaluating our exemplar modality. For all, we train on downsampled x4 images.

4.2. Comparison with the state-of-the-art

Baselines We compare with four baselines for few-shot image translation with $|\mathcal{T}| = 25$. We extensively evaluate on the most challenging Day \mapsto Night task, and provide insights and comparison for the two others tasks. We evaluate the impact of the few-shot image selection and of $|\mathcal{T}|$ in Sec. 4.5. For *general* image translation (*i.e.*, GERM-G), we compare against the recent FUNIT [28] and COCO-FUNIT [43], trained on $\mathcal{S} \mapsto \mathcal{A}_m$ and adapted to \mathcal{T} at inference. For *exemplar* image translation (*i.e.*, GERM-E), we compare to WCT² [56] used to transfer the style of the paired target condition to the source one. We also evaluate EGSC-IT [30]. The method is trained by merging \mathcal{A}_m and \mathcal{T} since it should be able to identify inter-domain variability, separating \mathcal{T} styles from \mathcal{A}_m [30]. To define metrics bounds, we also train our MUNIT [13] backbone on \mathcal{A}_m , on the full \mathcal{T} set and on \mathcal{T} with $|\mathcal{T}| = 25$. More comparisons with the backbone are in Sec. 4.5. We use the official code provided by the authors for all². More details on baselines are in supp.

Evaluation We compare qualitative results in Fig. 4. In Day \mapsto Night (Fig. 4a), even if the appearance of images in \mathcal{T} is partially transferred on translated images (e.g. road color, darker sky), FUNIT and COCO-FUNIT still strongly focus on textures of the anchor domains in \mathcal{A} (note, for example, how the street is similar to the anchor) which worsens the overall image realism. The same can be observed with EGSC-IT, where the hood of the ego-vehicle in anchor images (first column) is retained and significantly impacts visual results. While WCT² exhibits sharp results, it does

²For FUNIT [28] and COCO-FUNIT [43], we modify hyperparameters per authors suggestions obtained in private conversation to adapt to the ACDC and Dark Zurich datasets.

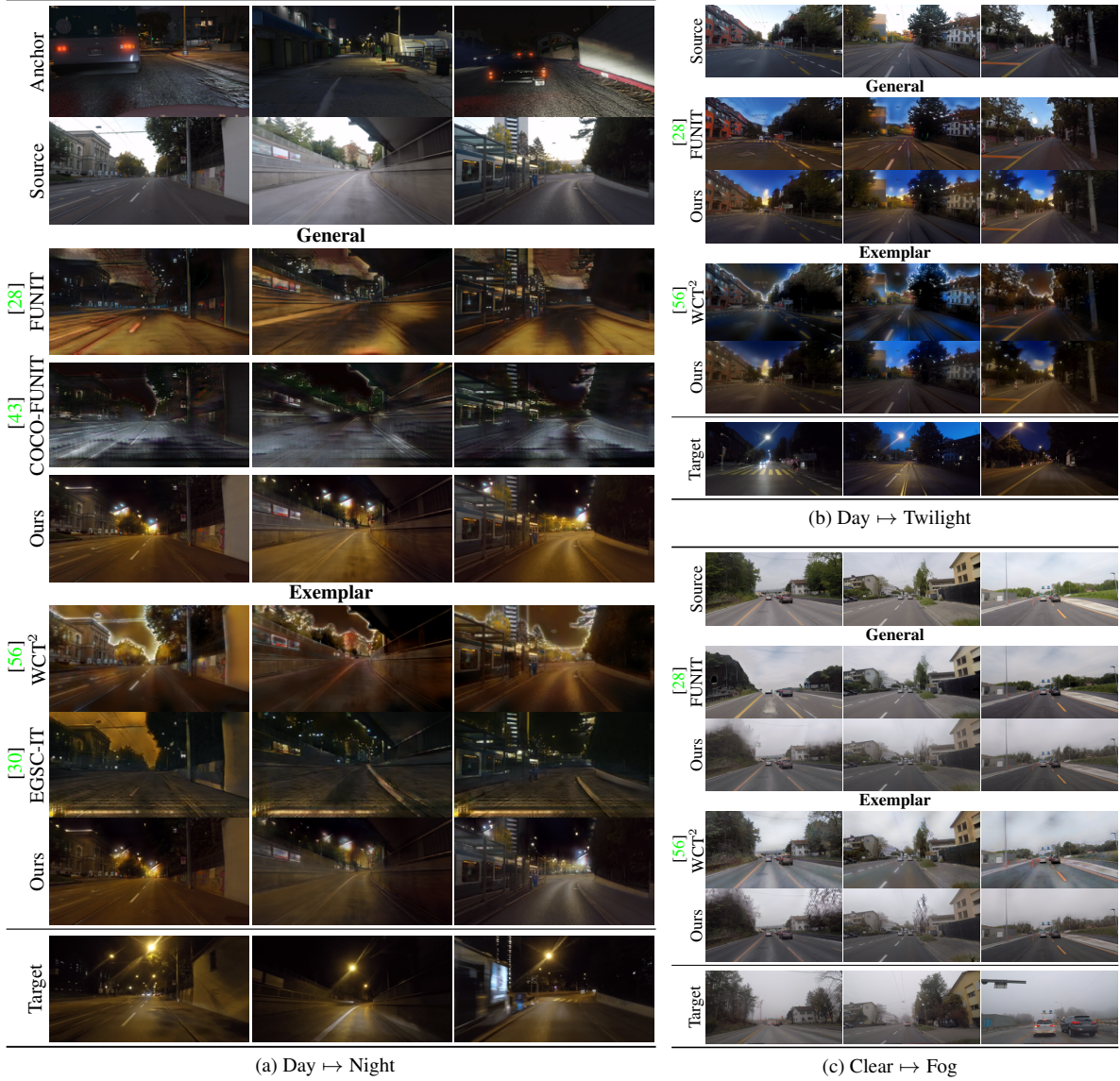


Figure 4. Qualitative evaluation and comparison with the state of the art. We evaluate the (a) Day \mapsto Night, (b) Day \mapsto Twilight, and (c) Clear \mapsto Fog tasks. In all cases, our approach extracts a *general* realistic representation of the few-shot target, and correctly reproduces the style of paired *exemplar* target images. In comparison, existing baselines either suffer from entanglement with the anchor domain (e.g. FUNIT, COCO-FUNIT, EGSC-IT) or from unrealistic artifacts (e.g. WCT²).

not correctly map the image context, being limited to appearance alignment which leads to artifacts (e.g. yellow sky with white halos). Our method generates significantly better results than the baselines in both the *general* and *exemplar* modalities, with evident differences in all three tasks: while the *general* appearance is consistent across test samples, each result adapts to its exemplar. For example, note how the overall sky colors (Day \mapsto Twilight, Fig. 4b) match the exemplar. Please note that Target images are unseen in training, thus GERM-E generalizes the few-shot learned exemplar behavior. The quantitative evaluation in Tab. 1 is coherent with

the qualitative results, as we always outperform baselines. We perform on par (*general*), or even better (*exemplar*) than the backbone trained on the entire set of 400 training images on Day \mapsto Night (Tab. 1a). This result shows that GERM-E (Sec. 3.3), as opposed to AdaIN exemplar style injection as in [13], improves modeling of the exemplar style.

4.3. Segmentation proxy

We exploit semantic segmentation to evaluate ManiFest for increasing robustness. In Fig. 5 we train HRNet [51] on Day \mapsto Night versions of Cityscapes translated with GERM-

Method	$ \mathcal{A}_m $	$ \mathcal{T} $	FID_{\downarrow}	$\text{LPIPS}_{\downarrow}$
MUNIT [13]	0	400	79.20	0.529
MUNIT [13]	3090	0	132.72	0.613
G	MUNIT [13]	0	25	91.61
	FUNIT [28]	3090	25	156.97
	COCOFUNIT [43]	3090	25	201.67
	Ours	3090	25	81.01
E	MUNIT [13]	0	400	87.71
	MUNIT [13]	3090	0	142.04
	MUNIT [13]	0	25	128.73
	EGSC-IT [30]	3090	25	106.68
E	WCT ² [56]	-	-	105.58
	Ours	3090	25	80.57
	Ours	3090	25	0.525

(a) Day \mapsto Night					
Method	$ \mathcal{A}_m $	$ \mathcal{T} $	FID_{\downarrow}	$\text{LPIPS}_{\downarrow}$	
G	FUNIT [28]	3090	25	69.53	0.511
	Ours	3090	25	63.15	0.510
E	WCT ² [56]	-	-	71.77	0.536
	Ours	3090	25	58.07	0.483

(b) Day \mapsto Twilight					
Method	$ \mathcal{A}_m $	$ \mathcal{T} $	FID_{\downarrow}	$\text{LPIPS}_{\downarrow}$	
G	FUNIT [28]	3090	25	122.4	0.580
	Ours	3090	25	89.57	0.520
E	WCT ² [56]	-	-	120.9	0.591
	Ours	3090	25	89.89	0.521

(c) Clear \mapsto Fog					

Table 1. Quantitative comparison with state of the art. We compare FID and LPIPS on the (a) Day \mapsto Night, (b) Day \mapsto Twilight and (c) Clear \mapsto Fog tasks, for both *general* (G) and *exemplar* (E) translations. Our approach outperforms all baselines on all tasks, while also being on par (G) or even outperforming (E) the MUNIT backbone trained on the full dataset for Day \mapsto Night in (a).

Model	mIoU % \uparrow	Acc. % \uparrow
Baseline (CS day)	12.93	45.15
MUNIT-S	17.21	54.67
MUNIT [13]	21.22	56.65
Ours - G	21.62	58.06
Ours - E	24.31	60.50
Oracle (ACDC night)	49.23	88.47

(a) Quantitative evaluation					

(b) Qualitative evaluation					

Figure 5. Segmentation on ACDC-night, for few-shot Day \mapsto Night translations ($|\mathcal{T}| = 25$). (a) We outperform the backbone in both configurations (*cf.* text) with noticeably better segmentation in (b).

G (unimodal) or GERM-E (multimodal), evaluating on the ACDC-night validation. As lower and upper bounds we train HRNet either on original Cityscapes (baseline) or on ACDC-night training set (oracle). Multimodality is impacting segmentation quality, so we compare both against MUNIT with a single style sampled (MUNIT-S) and in its default multimodal configuration (MUNIT). Fig. 5 shows we outperform both MUNIT settings thanks to our better domain modeling.

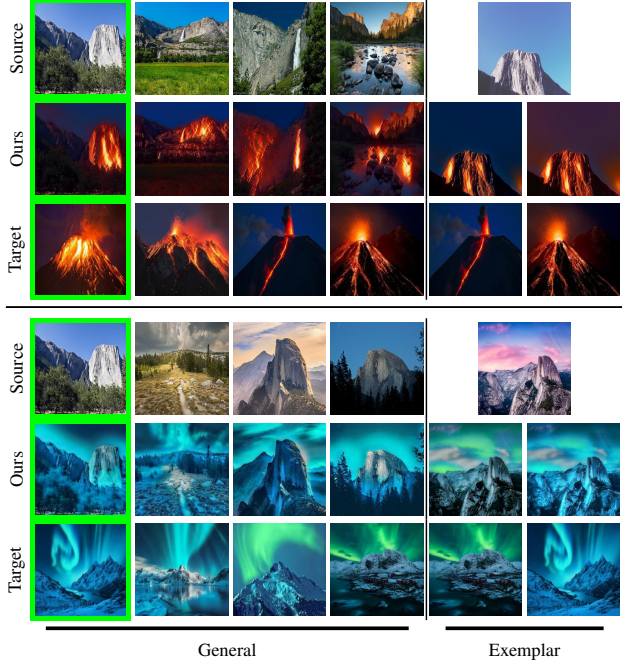


Figure 6. Qualitative evaluation for the Mountain \mapsto Volcano and Mountain \mapsto Aurora task. We retain contextual information by only partially mapping mountains to volcanoes and sky to auroras. In the green box we process the same image for ease of comparison. *Exemplar* results show how Ours conforms to Target (cols 5–6).

4.4. Rare few-shot scenarios

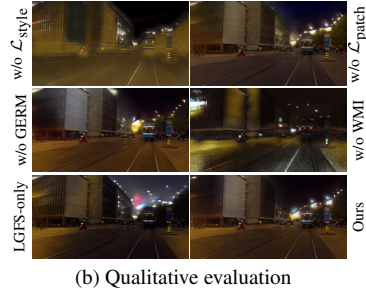
Few-shot plays its full role with conditions that are rare by nature, difficult or even dangerous to photograph, such as auroras or erupting volcanoes. Fig. 6 shows the capability of ManiFest to learn Mountain \mapsto Volcano or Day \mapsto Aurora, by taking as source and anchor the summer and winter Yosemite dataset [63] splits respectively. Each task uses only 4 images from Google Images as \mathcal{T} . We generate realistic erupting volcanoes or auroras starting from mountain images, with contextual understanding (Fig. 6, cols 1–4), where only one mountain is mapped to a volcano and auroras only partially cover the sky. Fig. 6 (cols 5–6) also demonstrate how exemplar characteristics are preserved.

4.5. Ablation studies

Architectural components We evaluate the contribution of each component in ManiFest (*cf.* Fig. 2, Sec. 3) using the Day \mapsto Night task in the *general* scenario, and report results in Fig. 7a. The impact of LGFS is studied by removing $\mathcal{L}_{\text{style}}$ or $\mathcal{L}_{\text{patch}}$, showing that both local *and* global guidance are improving translations. Removing the GERM from the training pipeline simultaneously precludes the *exemplar* behavior and worsens the performance, demonstrating the effectiveness of encoding complementary characteristics outside of the manifold spanned by \mathcal{A} . The benefit of WMI is evaluated

Component	FID \downarrow	LPIPS \downarrow
w/o $\mathcal{L}_{\text{style}}$	143.66	0.614
w/o $\mathcal{L}_{\text{patch}}$	93.42	0.566
w/o GERM	85.62	0.544
w/o WMI	101.57	0.589
LGFS-only	84.29	0.558
Ours	81.01	0.535

(a) Quantitative evaluation



(b) Qualitative evaluation

Figure 7. Ablation study for architectural components. (a) Removing each component individually lowers quantitative performances, which maps to (b) decreased visual quality in the generated images.

	\mathcal{S}	\mathcal{T}	\mathcal{A}_m	FID \downarrow	LPIPS \downarrow
Intra-dataset	ACDC-Day	ACDC-Night	Day	85.73	0.553
			Night	81.01	0.535
			Rain	81.38	0.549
			Snow	86.74	0.554
			Sunset	83.83	0.571
			All	83.71	0.547
Cross-dataset	ACDC-Day	DZ-Twilight	Day	64.19	0.505
			Night	63.15	0.510
			Rain	65.33	0.501
			Snow	64.09	0.513
			Sunset	63.78	0.504
			All	60.98	0.469
Intra-dataset	ACDC-Clear	ACDC-Fog	Day	89.57	0.520
			Night	91.79	0.520
			Rain	93.15	0.522
			Snow	90.28	0.524
			Sunset	90.11	0.525
			All	92.19	0.520
Cross-dataset	ACDC-Day	DZ-Twilight	Day	89.61	*
			Night	90.48	*
			Rain	89.47	*
			Snow	91.49	*
			Sunset	91.77	*
			All	85.15	*

* LPIPS is undefined given lack of paired images in the cross-dataset scenario.

Table 2. Study of the impact of anchor domains \mathbb{A} on the $\mathcal{S} \mapsto \mathcal{T}$ translations. The relatively stable performance across all tested anchors demonstrates the robustness of our method. Also, we test a multi-anchor setup by using all anchors (“All”). Note that LPIPS can be computed with pairs of matched images only (Sec. 4.1.1).

in two experiments. First, the “w/o WMI” setting applies the residual directly on the fake anchor images \tilde{s}_c , instead of the interpolated \tilde{s}_w as in Eq. (3). The worse performance relate to synthetic characteristics present in \tilde{s}_c (e.g. road texture in Fig. 7b). Second, “LGFS-only” directly uses the LGFS losses in substitution to \mathcal{L}_{adv} , without WMI and GERM components. While it only slightly worsens metrics, the impact on feature consistency is dramatic as shown in Fig. 7b, where the sky presents obvious artifacts and road trivially darkens.

Anchor selection We ablate the choice of anchor domain \mathbb{A} by selecting different conditions from the VIPER dataset, namely $\{\text{Day, Night, Rain, Snow, Sunset}\}$. In particular, we experiment on previous *intra-dataset* (\mathcal{S} and \mathcal{T} taken from the same dataset) tasks, as well as on a *cross-dataset* task

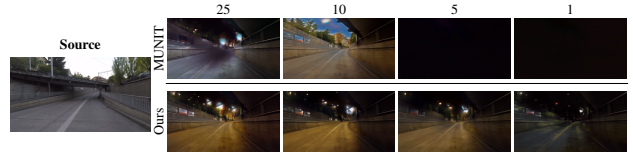


Figure 8. Comparison against MUNIT for varying $|\mathcal{T}|$: (a) qualitatively for the *general* scenario; as well as quantitatively for (b) *general* and (c) *exemplar*, outperforming it in any scenario.

GERM	Images	FID \downarrow		LPIPS \downarrow	
		25	15	5	1
G	25	82.95 \pm 2.95	0.541 \pm 1.85e-2		
	15	82.21 \pm 3.09	0.544 \pm 2.35e-2		
	5	83.11 \pm 2.49	0.535 \pm 2.24e-2		
	1	114.5 \pm 34.2	0.575 \pm 2.37e-2		
E	25	80.78 \pm 2.91	0.527 \pm 0.64e-2		
	15	80.55 \pm 2.85	0.527 \pm 1.07e-2		
	5	84.40 \pm 1.88	0.540 \pm 1.88e-2		
	1	114.3 \pm 33.5	0.575 \pm 2.40e-2		

Table 3. Ablation on variability by training on 4 few-shot configurations with 7 runs each. The number of images does not impact performance much except for the extreme one-shot scenario, where the network overfits to the seen styles. On average, the exemplar behavior performs better due to the style conditioning mechanism.

in which $\mathcal{S} = \text{ACDC-Day}$ and $\mathcal{T} = \text{DZ-Twilight}$. Results in Tab. 2 show how performance remains relatively stable across most anchors. This may seem counter-intuitive since one could, for example, expect that the “Rain” anchor would be a poor choice for the Day \mapsto Night task since rainy and night scenes look different. The results instead show that the WMI only encodes consistency in the transformation, and is thus robust to the choice of anchors. We also test a multi-anchor setup (“All” in Tab. 2), where $\mathbb{A} = \{\mathcal{A}_{\text{id}}, \text{Day, Night, Rain, Snow, Sunset}\}$. In general, more anchor domains improve performances, ranking either first or second in all cases for at least one metric, due to the additional information available for shaping the manifold in WMI. We hypothesize that multiple anchors helps identifying correspondences between \mathcal{S} and \mathcal{T} , benefiting especially the cross-dataset tasks.

Number of images and variability First we compare our Day \mapsto Night translations against MUNIT [13] for $|\mathcal{T}| = \{25, 20, 15, 10, 5, 1\}$, to understand the effects of few-shot training on the backbone network. Some qualitative *general* outputs are shown in Fig. 8a. While MUNIT overfits and creates unrealistic appearance (25–10 images) or collapse (5, 1 image), we output realistic transformations in all cases,



Figure 9. By enforcing multiple few-shot manifold deformations, we discover a realistic timelapse appearance comparable with CoMoGAN [39] and DNI-MUNIT [52] (all non few-shot).

even retaining the image context in the extreme one-shot scenario. This is confirmed by the FID and LPIPS in Figs 8b and 8c for the *general* and *exemplar* scenarios respectively.

In Tab. 3 we also study variability, evaluating FID and LPIPS for the *general* and *exemplar* cases for $|\mathcal{T}| = \{25, 15, 5, 1\}$ images reporting the results of 7 runs. Overall, the performance remains relatively constant with the exception of the one-shot setup, where despite realistic transfer, the metrics are penalized since the target image itself might not accurately represent the style distribution of the test set.

5. Extensions

5.1. Few-shot continuous manifolds

We investigate the use of ManiFest for performing continuous image translation as in CoMoGAN [39], by aiming to learn a transformation from $\mathcal{S} = \text{day}$ to $\mathcal{A}_m = \text{night}$ on the Waymo [47] dataset by generating realistically intermediate frontal sun / twilight conditions where we have only few images. Here, we consider *two* few-shot sets ($|\mathcal{T}| = 10$), each one associated to one set of learned weights (w^1, w^2) between identity and night anchors. Results are in Fig. 9, where we also perform comparably to DNI-MUNIT [52] and CoMoGAN which are trained with significantly more intermediate data (4721 vs 20). Please note that estimating w^1 and w^2 reorganizes the transformation realistically (*i.e.* Day \rightarrow Frontal sun \rightarrow Twilight \rightarrow Night) without prior knowledge on the order of few-shot set in the manifold. We evaluate mean rolling FID (mrFID) as in [39] and perform on par or better than baselines (for Model / StarGAN V2 / DNI - CycleGAN / DNI - MUNIT / CoMoGAN / *Ours* we get 195 / 177 / 155 / 144 / 145 / 145). Only CoMoGAN (mrFID 137) outperforms thanks to its physical guidance.

5.2. Anchor-based translation

The GERM module extracts residual information from encoded source images. We investigate the application of residuals on the anchor images themselves, by first translating from $\mathcal{A} \mapsto \mathcal{S}$ using our backbone cycle consistency, and afterwards re-encoding the fake image in a $\mathcal{S} \mapsto \mathcal{A}$

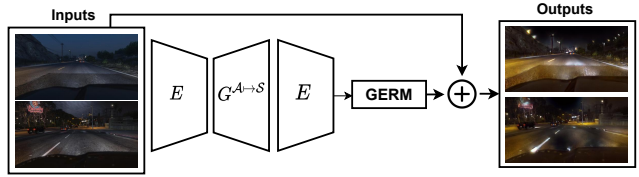


Figure 10. In the reconstruction cycle $\mathcal{A} \mapsto \mathcal{S} \mapsto \mathcal{A}$, we can inject the extracted residual with GERM on anchor images to perform an alternative $\mathcal{A} \mapsto \mathcal{T}$ transformation.

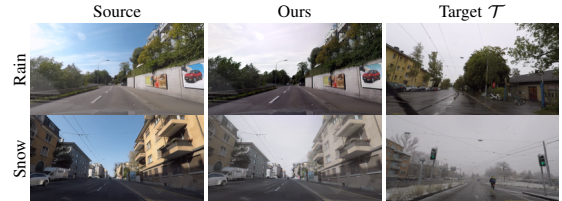


Figure 11. Illustration of limitations on the Clear \rightarrow Rain and Clear \rightarrow Snow tasks. While correctly approximating \mathcal{T} , our output images lack specific traits such as reflections or snowy sidewalks.

reconstruction *without retraining* (see Fig. 10). This shows how ManiFest simultaneously learns $\mathcal{S} \mapsto \mathcal{T}$ and acceptable $\mathcal{A} \mapsto \mathcal{T}$ transformations. The FID w.r.t ACDC-Night improves from 142 to 130 when applying the residual on the synthetic anchors, thus confirming their shift towards \mathcal{T} .

6. Discussion

In this paper we presented ManiFest, a framework for few-shot i2i which enables translating images to a single *general* style approximating the entire few-shot set (*e.g.*, for photo editing), or reproducing any specific *exemplar* from the set for more variability (*e.g.*, for domain adaptation).

Limitations The main limitation of ManiFest is the need to retrain for adapting to different few-shot sets, but the entire pipeline is shown to generalize sufficiently to reduce this need in the tested tasks. Another limitation is related to the local transformation capabilities of the network. We tested additional tasks as Clear \rightarrow Rain and Clear \rightarrow Snow using ACDC corresponding images (see Fig. 11). As visible, even if ManiFest correctly reproduces target images general appearance, it fails to render small but important traits for the scene realism such as reflections or snowy sidewalks. We hypothesize these features require additional contextual understanding to be rendered and propose to inject semantic guidance in ManiFest as future development.

Broader impact Even though face GANs are more susceptible to weaponization [46], any GAN risks misuse. By reducing the need for training data, our paper contributes to making these techniques more widely applicable. Promising solutions include digital authentication schemes. We urge readers to use our code for good only.

Acknowledgements This work was partially supported by the Service de coopération et d’action culturelle du Consulat général de France à Québec, and by Vislab Ambarella. It was performed using HPC resources from GENCI-IDRIS (Grant 2021-AD011012808).

References

- [1] Mohamed Abderrahmen Abid, Ihsen Heddhi, Jean-François Lalonde, and Christian Gagne. Image-to-image translation with low resolution conditioning. *arXiv*, 2021. [2](#)
- [2] Jie Cao, Luanxuan Hou, Ming-Hsuan Yang, Ran He, and Zhenan Sun. Remix: Towards image-to-image translation with limited data. In *CVPR*, 2021. [2](#)
- [3] Wei-Yu Chen, Yen-Cheng Liu, Zsolt Kira, Yu-Chiang Frank Wang, and Jia-Bin Huang. A closer look at few-shot classification. In *ICLR*, 2019. [2](#)
- [4] Anoop Cherian and Alan Sullivan. Sem-gan: Semantically-consistent image-to-image translation. In *WACV*, 2019. [2](#)
- [5] Yunjey Choi, Youngjung Uh, Jaejun Yoo, and Jung-Woo Ha. Stargan v2: Diverse image synthesis for multiple domains. In *CVPR*, 2020. [2, 4](#)
- [6] Marius Cordts, Mohamed Omran, Sebastian Ramos, Timo Rehfeld, Markus Enzweiler, Rodrigo Benenson, Uwe Franke, Stefan Roth, and Bernt Schiele. The cityscapes dataset for semantic urban scene understanding. In *CVPR*, 2016. [4](#)
- [7] Anthony Dell’Eva, Fabio Pizzati, Massimo Bertozzi, and Raoul de Charette. Leveraging local domains for image-to-image translation. In *VISAPP*, 2022. [2](#)
- [8] Yuki Endo and Yoshihiro Kanamori. Few-shot semantic image synthesis using stylegan prior. *arXiv*, 2021. [2](#)
- [9] Leon A Gatys, Alexander S Ecker, and Matthias Bethge. Image style transfer using convolutional neural networks. In *CVPR*, 2016. [2](#)
- [10] Martin Heusel, Hubert Ramsauer, Thomas Unterthiner, Bernhard Nessler, and Sepp Hochreiter. Gans trained by a two time-scale update rule converge to a local nash equilibrium. In *NeurIPS*, 2017. [4](#)
- [11] Hezhen Hu, Weilun Wang, Wengang Zhou, Weichao Zhao, and Houqiang Li. Model-aware gesture-to-gesture translation. In *CVPR*, 2021. [2](#)
- [12] Xun Huang and Serge Belongie. Arbitrary style transfer in real-time with adaptive instance normalization. In *ICCV*, 2017. [2, 3](#)
- [13] Xun Huang, Ming-Yu Liu, Serge Belongie, and Jan Kautz. Multimodal unsupervised image-to-image translation. In *ECCV*, 2018. [2, 3, 4, 5, 6, 7](#)
- [14] Phillip Isola, Jun-Yan Zhu, Tinghui Zhou, and Alexei A Efros. Image-to-image translation with conditional adversarial networks. In *CVPR*, 2017. [2](#)
- [15] Zhiwei Jia, Bodi Yuan, Kangkang Wang, Hong Wu, David Clifford, Zhiqiang Yuan, and Hao Su. Semantically robust unpaired image translation for data with unmatched semantics statistics. In *ICCV*, 2021. [2](#)
- [16] Liming Jiang, Changxu Zhang, Mingyang Huang, Chunxiao Liu, Jianping Shi, and Chen Change Loy. Tsit: A simple and versatile framework for image-to-image translation. In *ECCV*, 2020. [2](#)
- [17] Tero Karras, Miika Aittala, Janne Hellsten, Samuli Laine, Jaakko Lehtinen, and Timo Aila. Training generative adversarial networks with limited data. In *NeurIPS*, 2020. [2](#)
- [18] Hsin-Ying Lee, Hung-Yu Tseng, Qi Mao, Jia-Bin Huang, Yu-Ding Lu, Maneesh Singh, and Ming-Hsuan Yang. Drit++: Diverse image-to-image translation via disentangled representations. *IJCV*, 2020. [2](#)
- [19] Peilun Li, Xiaodan Liang, Daoyuan Jia, and Eric P Xing. Semantic-aware grad-gan for virtual-to-real urban scene adaptation. *BMVC*, 2018. [2](#)
- [20] Yijun Li, Chen Fang, Jimei Yang, Zhaowen Wang, Xin Lu, and Ming-Hsuan Yang. Universal style transfer via feature transforms. In *NeurIPS*, 2017. [2](#)
- [21] Yijun Li, Ming-Yu Liu, Xuetong Li, Ming-Hsuan Yang, and Jan Kautz. A closed-form solution to photorealistic image stylization. In *ECCV*, 2018. [2](#)
- [22] Yunsheng Li, Lu Yuan, and Nuno Vasconcelos. Bidirectional learning for domain adaptation of semantic segmentation. In *CVPR*, 2019. [1](#)
- [23] Yijun Li, Richard Zhang, Jingwan Lu, and Eli Shechtman. Few-shot image generation with elastic weight consolidation. In *NeurIPS*, 2020. [2](#)
- [24] Che-Tsung Lin, Yen-Yi Wu, Po-Hao Hsu, and Shang-Hong Lai. Multimodal structure-consistent image-to-image translation. In *AAAI*, 2020. [2](#)
- [25] Jianxin Lin, Yijun Wang, Tianyu He, and Zhibo Chen. Learning to transfer: Unsupervised meta domain translation. In *AAAI*, 2020. [2](#)
- [26] Jianxin Lin, Yingce Xia, Sen Liu, Shuxin Zhao, and Zhibo Chen. Zstgan: An adversarial approach for unsupervised zero-shot image-to-image translation. *Neurocomputing*, 2021. [2](#)
- [27] Ming-Yu Liu, Thomas Breuel, and Jan Kautz. Unsupervised image-to-image translation networks. In *NeurIPS*, 2017. [2](#)
- [28] Ming-Yu Liu, Xun Huang, Arun Mallya, Tero Karras, Timo Aila, Jaakko Lehtinen, and Jan Kautz. Few-shot unsupervised image-to-image translation. In *ICCV*, 2019. [1, 2, 4, 5, 6](#)
- [29] Fujun Luan, Sylvain Paris, Eli Shechtman, and Kavita Bala. Deep photo style transfer. In *CVPR*, 2017. [2](#)
- [30] Liqian Ma, Xu Jia, Stamatios Georgoulis, Tinne Tuytelaars, and Luc Van Gool. Exemplar guided unsupervised image-to-image translation with semantic consistency. In *ICLR*, 2019. [1, 2, 3, 4, 5, 6](#)
- [31] Xudong Mao, Qing Li, Haoran Xie, Raymond YK Lau, Zhen Wang, and Stephen Paul Smolley. Least squares generative adversarial networks. In *ICCV*, 2017. [4](#)
- [32] Sangwoo Mo, Minsu Cho, and Jinwoo Shin. Instagan: Instance-aware image-to-image translation. *ICLR*, 2019. [2](#)
- [33] Utkarsh Ojha, Yijun Li, Jingwan Lu, Alexei A Efros, Yong Jae Lee, Eli Shechtman, and Richard Zhang. Few-shot image generation via cross-domain correspondence. In *CVPR*, 2021. [1, 2](#)
- [34] Taesung Park, Alexei A Efros, Richard Zhang, and Jun-Yan Zhu. Contrastive learning for unpaired image-to-image translation. In *ECCV*, 2020. [2](#)
- [35] Taesung Park, Ming-Yu Liu, Ting-Chun Wang, and Jun-Yan Zhu. Semantic image synthesis with spatially-adaptive normalization. In *CVPR*, 2019. [1](#)

- [36] Taesung Park, Jun-Yan Zhu, Oliver Wang, Jingwan Lu, Eli Shechtman, Alexei A Efros, and Richard Zhang. Swapping autoencoder for deep image manipulation. In *NeurIPS*, 2020. 1
- [37] Or Patashnik, Dov Danon, Hao Zhang, and Daniel Cohen-Or. Balagan: Cross-modal image translation between imbalanced domains. In *CVPR Workshops*, 2021. 2
- [38] Fabio Pizzati, Pietro Cerri, and Raoul de Charette. Model-based occlusion disentanglement for image-to-image translation. In *ECCV*, 2020. 2
- [39] Fabio Pizzati, Pietro Cerri, and Raoul de Charette. CoMoGAN: continuous model-guided image-to-image translation. In *CVPR*, 2021. 2, 8
- [40] Fabio Pizzati, Pietro Cerri, and Raoul de Charette. Guided disentanglement in generative networks. *arXiv*, 2021. 2
- [41] Pierluigi Zama Ramirez, Alessio Tonioni, and Luigi Di Stefano. Exploiting semantics in adversarial training for image-level domain adaptation. In *IPAS*, 2018. 2
- [42] Stephan R Richter, Zeeshan Hayder, and Vladlen Koltun. Playing for benchmarks. In *ICCV*, 2017. 4
- [43] Kuniaki Saito, Kate Saenko, and Ming-Yu Liu. COCO-FUNIT: Few-shot unsupervised image translation with a content conditioned style encoder. In *ECCV*, 2020. 1, 2, 4, 5, 6
- [44] Christos Sakaridis, Dengxin Dai, and Luc Van Gool. Map-guided curriculum domain adaptation and uncertainty-aware evaluation for semantic nighttime image segmentation. *T-PAMI*, 2020. 1, 4
- [45] Christos Sakaridis, Dengxin Dai, and Luc Van Gool. ACDC: The adverse conditions dataset with correspondences for semantic driving scene understanding. In *ICCV*, 2021. 4
- [46] Hannah Smith and Katherine Mansted. Weaponised deep fakes: national security and democracy. 2020. 8
- [47] Pei Sun, Henrik Kretzschmar, Xerxes Dotiwalla, Aurelien Chouard, Vijaysai Patnaik, Paul Tsui, James Guo, Yin Zhou, Yuning Chai, Benjamin Caine, et al. Scalability in perception for autonomous driving: Waymo open dataset. In *CVPR*, 2020. 8
- [48] Hao Tang, Dan Xu, Yan Yan, Jason J Corso, Philip HS Torr, and Nicu Sebe. Multi-channel attention selection gans for guided image-to-image translation. In *CVPR*, 2019. 2
- [49] Lisa Torrey and Jude Shavlik. Transfer learning. In *Handbook of research on machine learning applications and trends: algorithms, methods, and techniques*. IGI global, 2010. 2
- [50] Maxime Tremblay, Shirsendu Sukanta Halder, Raoul de Charette, and Jean-François Lalonde. Rain rendering for evaluating and improving robustness to bad weather. *IJCV*, 2020. 2
- [51] Jingdong Wang, Ke Sun, Tianheng Cheng, Borui Jiang, Chaorui Deng, Yang Zhao, Dong Liu, Yadong Mu, Mingkui Tan, Xinggang Wang, Wenyu Liu, and Bin Xiao. Deep high-resolution representation learning for visual recognition. *TPAMI*, 2019. 5
- [52] Xintao Wang, Ke Yu, Chao Dong, Xiaou Tang, and Chen Change Loy. Deep network interpolation for continuous imagery effect transition. In *CVPR*, 2019. 8
- [53] Yaxing Wang, Salman Khan, Abel Gonzalez-Garcia, Joost van de Weijer, and Fahad Shahbaz Khan. Semi-supervised learning for few-shot image-to-image translation. In *CVPR*, 2020. 2
- [54] Yaxing Wang, Hector Laria Mantecon, Joost van de Weijer, Laura Lopez-Fuentes, and Bogdan Raducanu. Transferi2i: Transfer learning for image-to-image translation from small datasets. In *ICCV*, 2021. 2
- [55] Wayne Wu, Kaidi Cao, Cheng Li, Chen Qian, and Chen Change Loy. Transgaga: Geometry-aware unsupervised image-to-image translation. In *CVPR*, 2019. 2
- [56] Jaejun Yoo, Youngjung Uh, Sanghyuk Chun, Byeongkyu Kang, and Jung-Woo Ha. Photorealistic style transfer via wavelet transforms. In *ICCV*, 2019. 2, 4, 5, 6
- [57] Xiaoming Yu, Yuanqi Chen, Shan Liu, Thomas Li, and Ge Li. Multi-mapping image-to-image translation via learning disentanglement. In *NeurIPS*, 2019. 2
- [58] Fangneng Zhan, Yingchen Yu, Kaiwen Cui, Gongjie Zhang, Shijian Lu, Jianxiong Pan, Changgong Zhang, Feiying Ma, Xuanlong Xie, and Chunyan Miao. Unbalanced feature transport for exemplar-based image translation. In *CVPR*, 2021. 2
- [59] Pan Zhang, Bo Zhang, Dong Chen, Lu Yuan, and Fang Wen. Cross-domain correspondence learning for exemplar-based image translation. In *CVPR*, 2020. 2
- [60] Richard Zhang, Phillip Isola, Alexei A Efros, Eli Shechtman, and Oliver Wang. The unreasonable effectiveness of deep features as a perceptual metric. In *CVPR*, 2018. 4
- [61] Shengyu Zhao, Zhijian Liu, Ji Lin, Jun-Yan Zhu, and Song Han. Differentiable augmentation for data-efficient gan training. *NeurIPS*, 2020. 2
- [62] Chuanxia Zheng, Tat-Jen Cham, and Jianfei Cai. The spatially-correlative loss for various image translation tasks. In *CVPR*, 2021. 2
- [63] Jun-Yan Zhu, Taesung Park, Phillip Isola, and Alexei A Efros. Unpaired image-to-image translation using cycle-consistent adversarial networks. In *CVPR*, 2017. 2, 6
- [64] Jun-Yan Zhu, Richard Zhang, Deepak Pathak, Trevor Darrell, Alexei A Efros, Oliver Wang, and Eli Shechtman. Toward multimodal image-to-image translation. In *NeurIPS*, 2017. 2
- [65] Peihao Zhu, Rameen Abdal, Yipeng Qin, and Peter Wonka. Sean: Image synthesis with semantic region-adaptive normalization. In *CVPR*, 2020. 2
- [66] Zhen Zhu, Zhiliang Xu, Ansheng You, and Xiang Bai. Semantically multi-modal image synthesis. In *CVPR*, 2020. 2